TITLE: Capacitive sensing of an amphetamine drug precursor in aqueous samples: Application of novel molecularly imprinted polymers for benzyl methyl ketone detection.

Authors: De Rycke E., Trynda A., Jaworowicz M., Dubruel P., De Saeger S., Beloglazova N.

In: Biosensors and Bioelectronics 172, article 112773, 2021

Optional: https://doi.org/10.1016/j.bios.2020.112773

Capacitive sensing of an amphetamine drug precursor in aqueous samples: Application of novel molecularly imprinted polymers for benzyl methyl ketone detection.

Esther De Rycke[1,2]*, Anna Trynda[3], Magdalena Jaworowicz[3], Peter Dubruel[2], Sarah De Saeger[1,4]**, and Natalia Beloglazova[1,5]**

[1] *Centre of Excellence in Mycotoxicology and Public Health, Ghent University, Department of Bioanalysis, Ottergemsesteenweg 460, B-9000 Ghent, Belgium.*

[2] *Polymer Chemistry & Biomaterials Research Group, Centre of Macromolecular Chemistry (CMaC), Department of Organic and Macromolecular Chemistry, Ghent University, Krijgslaan 281, Building S4-Bis, B-9000 Ghent, Belgium.*

[3] *Central Forensic Laboratory of the Police, Warsaw, Poland.*

[4] *Department of Biotechnology and Food Technology, Faculty of Science, University of Johannesburg, Doornfontein Campus, Gauteng, South Africa*

[5] *Nanotechnology Education and Research Center, South Ural State University, 454080 Chelyabinsk, Russia.*

* Corresponding author: esther.derycke@ugent.be

** Authors contributed equally to this work

Abstract

Highly selective molecularly imprinted polymers (MIPs) towards benzyl methyl ketone (BMK) were synthesized for application as recognition elements in a capacitive sensor. A computational approach was employed to select the most appropriate monomers and cross-linkers. Using the selected compounds, different polymerization techniques and protocols were compared in order to study the effect on the MIP performance and characteristics. MIPs synthesized by bulk polymerization using itaconic acid and 1-vinylimidazole as monomers and p-divinylbenzene as cross-linker possess the highest affinity towards the target analyte. Prior to capacitive analysis, the developed particles were immobilized on the surface of gold transducers using tyramine as a linker. The validity of the developed sensor was checked by the BMK detection in spiked tap water and real water samples. A linear working range from 50-1000 µM was found while the limit of detection (LOD) was determined to be 1 µM in tap water. To the best of our knowledge, both the developed MIPs towards BMK and the electrochemical sensor for its detection have not been published or marketed to date.

Key words

Amphetamine type stimulants, benzyl methyl ketone, capacitive sensor, molecularly imprinted polymers, environmental analysis.

1. Introduction

Illicit drugs and their abuse have been a long-standing and global problem, irrespective of the country's economic situation (UNDCP, 1995). According to the United Nation Office on Drugs and Crime (UNODC) drug report from 2017, a quarter billion people used drugs at least once that year whereof almost 30 million people suffered from problematic drug abuse and/or a drug disorder (United Nations Office on Drugs and Crime, 2017). Every year, approximately 250.000 deaths worldwide are drug-related, and the total global value of illicit drug markets is estimated at 332 billion dollars (United Nations Office on Drugs and Crime, 2007). Although cannabis remains the most popular drug, the amount of amphetamine-type stimulants (ATS) users increased dramatically since the last decade (UNODC, 2018). ATS refer to a group of drugs whose main principal members include amphetamine (AMP), methamphetamine (MA), 3,4-methylenedioxymethamphetamine (MDMA), methcathinone, methylphenidate, and fenethylline. For ATS detection, also their precursors (benzyl methyl ketone (BMK), α-phenylacetoacetonitrile (APAAN), etc.), impurities (4-methyl-5-phenyl pyrimidine (4M5PP), N,N-di-(β-phenylisopropyl)amine (DPIA), etc.) and intermediates (N-formyl amphetamine (NFA)) are interesting to monitor (Appendix A) (UNODC, 2018). ATS can be snorted, smoked, injected or used rectally and possess hallucinogenic properties. They can be easily synthesized from inexpensive precursors and the production can be efficiently scaled up to an industrial level. The most common way to produce ATS is through the Leuckart synthesis (Aalberg et al., 2005; Hauser et al., 2018). In the first step of this two-step process, BMK is converted into the amine NFA by adding ammonium formate or a mixture of ammonia and formic acid. This reaction takes place at a temperature of 180-195°C and a pH of approximately 5. NFA hydrolyses further at a temperature of 90-125°C in the presence of a strong acid to the corresponding amphetamine salt. This salt is converted to the amphetamine free base by adding an alkaline compound such as sodium hydroxide which alters the pH to 9-14 depending on the concentration of the alkaline (Hauser et al., 2018). The importance of the detection of ATS, including its precursors and derivatives, is indispensable: it can identify adults in need and check-up on ex-addicts (Warner et al., 2013), examine the purity of drugs and identify new types of drugs (Darke et al., 2002), determine the cause of death post mortally (Lehrmann et

al., 2009), map the use, distribution and transport of illicit drugs and reduce environmental pollution (Groeneveld et al., 2015; Zuccato et al., 2008). Although research for electrochemical detection of illicit drugs is quite common in biological matrices like urine and blood, environmental analysis in water systems is rather limited.

So far, ATS are mainly detected by chromatography, both liquid and gas (De Rycke et al., 2020; Fernández et al., 2004; Kala et al., 2008; Lurie, 1997). These procedures are known for their high accuracy and low limits of detection (LODs). The expensive- and time- consuming sample pre-treatment/extraction procedures, the need for expensive analytical devices and highly trained personnel, and the use of large quantities of organic solvents limit their application. Electrochemical sensors show great potential to tackle the abovementioned challenges due to their rapidity, robustness, simplicity, high sensitivity, user friendly interfaces and straight forward readouts, low costs and possibility for miniaturization (Labib et al., 2010, 2009). Since the last decades, capacitive sensors became a popular tool for the ultrasensitive (up to picomolar) detection of low molecular organic compounds (Liu et al., 2014; Teeparuksapun et al., 2010). Furthermore, this technique does not require sample pretreatment or large sample volumes. High-throughput screening is in reach given the short analysis time and the real-time data processing (Chambers et al., 2002; Zhang et al., 2012). Multiple capacitive sensing systems were previously reported using natural and artificial recognition elements on the transducers, mostly gold electrodes (Lenain et al., 2015; Liu et al., 2014; Teeparuksapun et al., 2010). Natural recognition elements, such as antibodies and aptamers, are very specific and sensitive, but are prone to functionality loss in harsh conditions, such as changes in temperature and pH, potential presence of algae, human waste, etc. Their limited tolerance to matrix changes, and to the presence of other substances (detergents, sweeteners) or organic solvents represent major drawbacks (Usami et al., 1996). To overcome these challenges, molecularly imprinted polymers (MIPs) will be used in this study as artificial recognition elements. They are easier to produce in a reproducible manner, less expensive and more robust. Molecular imprinting is a technology in which a target molecule is used as a template to form a polymer matrix, which can subsequently rebind this template in a selective fashion from a mixture of other compounds. The recognition process is similar to the classic “key-lock” interaction of an antibody, therefore MIPs are often nicknamed as "artificial antibodies". Although they have lower dissociation constant (K_D) values (microrange) than antibodies and aptamers, MIPs are favored for applications in environmental analysis where any biological receptor can degrade, denature or lose their affinity (Vasapollo et al., 2011).

To the best of our knowledge, this is the first manuscript describing MIPs towards BMK and one of a few works devoted to electrochemical MIP-based detection of ATS. Indeed, a highly sensitive, MIP-based capacitive sensor was developed by our group to monitor trace amounts of NFA in aqueous samples with a linear working range of 50-250 µM and an LOD of 50 µM (Graniczkowska et al., 2016). More recently, a square wave voltammetric sensor, was developed for MDMA detection in blood serum and urine. Therefore, MIPs were directly electropolymerized on a screen printed carbon electrode using *ortho*-phenylenediamine as monomer, chosen after computational (density functional theory (DFT)) calculation. A linear range was found up to 0.2 mM with an LOD of 0.79 µM (Couto et al., 2019). Furthermore, the use of MIPs for ATS detection in other types of sensors such as optical, gravimetric, acoustic, etc. is rather limited (Arenas et al., 2010; Masteri-Farahani et al., 2020; Romero Guerra et al., 2009). The majority of reported MIPs related to ATS monitoring is used in solid phase extraction, as pre-concentration or pretreatment step for subsequent chromatographic detection (Ahmadi et al., 2011; Djozan et al., 2012; Lowdon et al., 2018; Xiao et al., 2018). In the last years, with the rapid development of *in-silico* simulation, MIP synthesis is assisted by rational design of the polymer system through computational chemistry (Gholivand et al., 2012; Subrahmanyam and Piletsky, 2009; Yao et al., 2008). This computer simulation helps in determining the optimal functional monomer and optimizing the synthesis conditions. In the present manuscript, modeling was used to select the most optimal monomer(s) and cross-linker. Different polymerization techniques and protocols were compared in order to study a possible effect on the MIP characteristics and performance. MIP performance was investigated by liquid chromatography tandem mass spectrometry (LC-MS/MS). The most promising MIPs were further characterized using dynamic light scattering (DLS), thermogravimetric analysis (TGA), and optical microscopy. Template removal was checked by gas chromatography mass spectrometry (GC-MS) and TGA. MIP particles were immobilized on the gold transducers using tyramine as a linker. The success of this process was checked by cyclic voltammetry (CV), and scanning electron microscopy (SEM). The affinity, cross-reactivity, pH dependency, repeatability and reproducibility were investigated by analysis of spiked water samples. The validity was checked by the analysis of water samples. To the best of our knowledge, both the developed MIPs towards BMK and the electrochemical sensor for its detection have not been published or marketed to date.

2. Materials and methods

2.1 Materials

Chloroform (98%) was purchased from Novolab (Geraardsbergen, Belgium). Methanol (MeOH, LC-MS grade) was obtained from Biosolve BV (Valkenswaard, Netherlands), acetone was supplied by Fiers (Kuurne, Belgium), and absolute ethanol (EtOH, Analar Normapure) by VWR International (Leuven, Belgium). Sulfuric acid (95–97%), potassium dihydrogen phosphate (KH_2PO_4, p.a.), and potassium chloride (KCl, p.a.) were purchased from Merck (Darmstadt, Germany). Azobisisobutyronitrile (AIBN, 98%), dipotassium hydrogen phosphate (K_2HPO_4, ≥98%), p-divinylbenzene (DVB), 1-dodecanethiol (98%), ethylene glycol dimethacrylate (EGDMA, 98%), hydroxyethyl methacrylate (HEMA), hydrogen peroxide ($H2O_2$, 30 wt%), 2-mercaptobenzimidazole (2-MBI, 98%), methacrylic acid (MAA, 99%), poly(vinyl alcohol) (PVA, M_w 146.000-186.000, 99+% hydrolysed), potassium ferricyanide ($K_3[Fe(CN)_6]$, ≥99.0%), styrene (≥99%), trimethylamine (≥99%), trimethylolpropane trimethacrylate (TRIM, 99%), tyramine (99%), and 1-vinylimidazole were purchased from Sigma Aldrich (Bornem, Belgium). Disolol was purchased from Chem Lab (Zedelgem, Belgium). Standards of APAAN, NFA, 4M5PP, AMP base (AMP.OH), and BMK, were kindly provided by Bundeskriminalamt (Wiesbaden, Germany). Standard of amphetamine hydrochloride (AMP.HCl) was purchased from Lipomed AG (Arlesheim, Switzerland). Ultrapure water was obtained with the arium® pro system from Sartorius (Schaarbeek, Belgium).

The automated flow injection sensing system (Appendix B) and gold working electrodes were provided by CapSenze AB (Lund, Sweden). A PGSTAT2014 compact potentiostate/galvanostate was used to perform CV, a glassy carbon counter electrode and an Ag/AgCl reference electrode were bought from Metrohm (Antwerp, Belgium). DLS measurements were performed using a Zetasizer Nano series from Malvem Instruments (Worcestershire, UK). Optical measurements were performed by a SEM of Phenom (Eindhoven, the Netherlands) and an Axiotech 100, Axiocam 105 optical microscope from (Carl) Zeiss (Göttingen, Germany). TGA was done with a TGA Q50 of Waters (Brussels, Belgium). Batch rebinding studies were performed using an Acquity UPLC system coupled to a Waters Xevo® TQ-S triple quadrupole mass spectrometer (Waters Technologies, Zellik, Belgium). Masslynx and Targetlynx software 4.1 (Waters Corp., Milford, MA, USA) were used for data acquisition and processing. Chromatographic separation was performed using an Acquity UPLC HSS T3 (1.8 m x 2.1 x 100 mm) column (Waters, Milford, MA, USA). GC-MS measurements were performed using GC-MS Triple Quadrupole 7890B/7000C, and a HP5MS

capillary column (30 m length, 0.25 mm diameter, film thickness 0.25 µm with a pre-column of 3 m length, 0.25 mm diameter and film thickness of 0.10 µm) of Agilent Technologies Company (California, USA).

2.2 MIP modelling

Template–monomer interactions were modelled with the Spartan '16 software (California, United States) using a density functional (DFT) method with the hybrid Becke three-parameter B3LYP exchange correlation functional, and 6-311+G** basis set. BMK was chosen as the template for the MIP synthesis. After optimisation of the three-dimensional structures of the template, monomers, and template-monomer complexes, the ground state energy was calculated according to the local minima. The binding energy was calculated according to the following generic formula:

$$\Delta E_{binding} = E_{complex} - E_{template} - \sum (E_{monomers})$$

where $\Delta E_{binding}$ is the binding energy, $E_{complex}$ the energy of a template-monomer(s) complex, $E_{template}$ and $E_{monomer(s)}$ the energies of the template and monomer(s) respectively.

2.3 Bulk synthesis of BMK-MIPs

For the synthesis of MIPs towards BMK, different protocols and techniques were compared such as *in-situ*-, direct-, emulsion and bulk polymerisation. The protocol mentioned below represents the protocol for the synthesis of the most performing MIPs towards BMK. Other protocols can be found in detail in Appendix D. AIBN (50 mg) was dissolved in the porogen, DMF (2.65 mL). The template (BMK) and selected functional monomers (itaconic acid and 1-vinylimidazole) were added. After sonication for 5 minutes, the cross-linking agent (DVB) was added in a template/functional monomer/co-monomer/cross-linker molar ratio of 1/2/2/6. The pre-polymerization mixture was flushed with nitrogen for 5 minutes and sealed off. The polymerization occurred under UV light (λ = 365 nm, 150 mW cm^{-2}) for 20 minutes after which the mixture was left in an oil bath at 80 °C for 3h. The obtained monolith was crushed and sieved wetly. The template was removed by rinsing the obtained MIPs with a MeOH/acetic acid (95/5, v/v) solution for 48 h in a Soxhlet extractor. Non-imprinted polymers (NIPs) were synthesized via the same protocols, but in absence of the template. The obtained particles were characterized by LC-MS/MS, DLS, TGA, optical microscopy, and SEM.

2.4 Gold electrode immobilization of MIP/NIP beads

Prior to MIP immobilization, the gold electrode surface was cleaned to remove protective coatings and dust particles. Therefore, the gold working electrodes were sequentially

submerged and sonicated for 15 minutes in acetone, absolute ethanol, and piranha solution (H_2SO_4/H_2O_2; 3/1, v/v). Between each step, the electrode was rinsed with UPW and disolol and dried under a stream of nitrogen.

Five mg of MIP/NIP particles were suspended in 10 mL of a 10 mM conductive tyramine solution. To this end, 0.0137 g (0.100 mmol) tyramine was dissolved in 2.5 mL ethanol and further diluted with 7.5 mL of 10 mM phosphate-bisulphate buffer (PBS, KH_2PO_4/K_2HPO_4 in UPW, pH = 7.2). A gold electrode was fixed in a reaction cell and 300 µL of the above mentioned suspension was added. The beads were allowed to sediment for 15 minutes, settling down to close proximity of the surface. The gold electrode served as the working electrode, the reaction cell further included a platinum reference and a platinum auxiliary electrode that allowed anionic electro-oxidation of tyramine by varying the potential. After 15 potential sweeps at a potential from 0 to 1.5 V and a scan rate of 50 mV s^{-1}, a polytyramine network with incorporated MIP/NIP was formed. The functionalized electrodes were subsequently placed in 10 mM 1-dodecanethiol in ethanol for 20 minutes to insulate the remaining pinholes on the gold surface. To assure the success of the immobilization, CV was performed in 10 mM $K_3[Fe(CN)_6]$ in 0.1 M KCl in H_2O, both before and after immobilization.

2.5 Capacitive measurements

Capacitive analyses involved two steps, the regeneration and the sampling step (Appendix B). During regeneration, 250 µL of regeneration buffer, consisting of MeOH/phosphate-biphosphate buffer/trimethylamine (47.5/47.5/5, v/v/v), was pumped through the flow cell. The regeneration buffer cleaned the active surface of the functionalized gold electrode and assured that the MIP was free for (re)binding by breaking the bonds between template and MIP. Afterwards, running buffer (phosphate-biphosphate buffer, pH = 7.2) was used for flushing, causing the baseline to return to its initial, stable state. In the sequential sampling step, 250 µL of sample was added, giving the opportunity for the binding event between MIP and target analyte to occur. Once again, running buffer was pumped to remove unbound compounds from the flow cell. All fluidics were pumped at a flow rate of 1.67 mL min^{-1}. The binding event typically resulted in a decrease of the observed capacitance whereas the size of the drop was directly proportional to the analyte concentration. To calculate the capacitive drop, the difference between the average of 5 data points prior and after the sampling step was taken.

3. Results and discussion

The aim of the present research is to develop MIPs, which are used as recognition elements for the capacitive sensing of BMK in aqueous samples. In the first step, modelling was applied to select the most optimal monomers and cross linkers. These compounds were used in different ratios and polymerisation techniques in order to find the MIPs with the highest affinity towards the target analyte. After full characterization, the most promising MIPs were immobilized on gold electrodes. In order to validate the developed sensing system, the affinity, cross-reactivity, pH dependency, repeatability and reproducibility were investigated by the analysis of spiked water samples, followed by the analysis of several real samples.

3.1 Optimization of MIP synthesis through modelling

The interaction between the template and the functional monomer(s) is one of the most important characteristics since it influences the specific recognition ability of the obtained MIP particles. Using molecular modelling, the most promising functional monomers for the template can be selected in this way reducing the number of experiments. The selection of the polymerization technique and the different reagents were based on both literature research and practical experience.

For the synthesis of MIPs toward BMK, different monomers were compared including basic monomers (methacrylic acid (MAA), acrylamide and itaconic acid), aromatic monomers (styrene, 4-hydroxysterene and 4-vinylbenzene) to enable π-π stacking, and amine-containing compounds (diethylaminoethyl methacrylate), of which some are aromatic (4-aminostyrene, 1-(4-ethenylphenyl)-3-phenylurea, 2-(diethylamino)ethylstyrene) to enable hydrogen bond formation with the carboxyl functionality of the template. To choose the most optimal monomer(s), computational analysis was used. The binding energy of a template-monomer complex was compared to the free binding energy of both components separately, and the system with the most negative difference indicated the most stable combination. The selection of the optimal cross-linker was realized in a different way. A lower binding (indicated by a more positive or a less negative value) between the cross-linker and the template is preferable since it is able to generate MIPs with a lower non-specific binding, a higher imprinting factor, and therefore a higher specificity. In this study, the geometries were computed, and the binding energies were calculated by the Spartan ’16 software using DFT B3LYP with a 6-311+G** basis set. The simulation results showed that styrene, itaconic acid, and 1-vinylimidazole formed the most stable complex (-26.29; -18.19; -17.92 kJ mol^{-1} respectively) with the template

(ratio 1:1) via electrostatic non-covalent interactions. The cross-linkers DVB and EGDMA (3.28 and 2.72 kJ mol^{-1}) were the most promising. The binding energies of BMK with all tested monomers and cross-linkers (molar ratio 1:1) are summarized in Appendix C.

With this knowledge, different ratios were tested by modelling as well as in lab experiments to determine the optimal ratio between the template and monomer(s). The results of the modelling are summarized in Table 1. An increase in the template/monomer ratio, did not result in extra stability. Indeed, positive binding energies were found at ratios of 1:2, 1:3 and 1:4. In a next step, two monomers were combined and tested. This resulted in negative values of the binding energies. Therefore, several of these combinations were tested in lab experiments.

Table 1. Binding energies of monomers and the template BMK, in different molar ratios. (Abbreviations: BMK, benzyl methyl ketone; IA, itaconic acid; STY, styrene; VI, vinylimidazole.)

Complex	**Ratio**	**kJ mol^{-1}**	**Complex**	**Ratio**	**kJ mol^{-1}**
BMK - STY	1:2	3.24	BMK - STY - IA	1:1:1	-20.74
	1:3	1.77		1:2:2	-15.60
	1:4	2.40	BMK - STY - VI	1:1:1	-18.27
BMK - VI	1:2	20.89		1:2:2	-36.80
	1:3	35.74	BMK - IA - VI	1:1:1	-37.51
	1:4	47.59		1:2:2	-34.55
BMK - IA	1:2	-10.64			
	1:3	10.32			
	1:4	-87.09			

3.2 MIP synthesis

Once the monomers and the cross-linking agent were selected through modelling, different polymerization techniques and protocols, using different ratios of the compounds, were compared. AIBN was chosen as an initiator as it allows both thermal and photochemical initiation. The detailed protocols can be found in Appendix D.

3.2.1 Emulsion polymerization

The particles obtained from the first MIP batches obtained by emulsion polymerization were of a large size (< 1 mm) as measured by DLS. Further optimisation of the protocol did not lead to any significant size reduction. After washing and drying, the particles were immobilised on the gold working electrodes using tyramine as a linker. The capacitive baseline was highly unstable with values ranging between 0 and 1400 nF (Appendix Figure D.1). These fluctuations could be caused by an incomplete coverage of the gold electrode due to the large size of the particles. A high baseline stability is a prerequisite to enable evaluation of a capacitive drop (in nF) during capacitive sensing of samples. The observed fluctuation was not appropriate for use in a sensor and emulsion polymerization was therefore excluded from further use.

3.2.2 Bulk polymerization

Bulk polymerization is the easiest, most straight-forward, and reproducible synthesis technique where after polymerization, the obtained monolith is crushed and sieved until particles with the desired size are obtained. In the next step, these particles were immobilized on the gold working electrodes using tyramine as a linker.

Different synthesis protocols were tested in which itaconic acid and styrene or itaconic acid and 1-vinylimidazole were used as co-monomer combinations (Appendix D.2). AIBN was used as an initiator, and DVB or EGDMA were tested as cross-linkers. Various molar ratios of the template/functional monomer/co-monomer/cross-linker were tested, such as 1/2/2/6, 1/2/2/16, and 1/2/2/20, or 1/4/16 and 1/4/20 in absence of a co-monomer. The obtained monoliths were crushed, wetly sieved, and washed by Soxhlet. The particles were characterized by DLS indicating sizes in the hundreds of nanometers range.

3.2.3 *In-situ* and direct polymerization

In order to perform capacitive sensing, the obtained MIP particles from bulk and emulsion polymerisation were sequentially immobilized on the surface of a gold electrode. To facilitate this procedure and reduce the amount of production steps, *in-situ* and direct polymerization on the gold electrode surface were tested as well.

The two synthetic approaches for *in-situ* polymerization are described in detail in Appendix D.3. The first protocol used an electroactive monomer 2-MBI (Appendix Figure D.2) that could copolymerize with the template on the electrode surface. This protocol did not include any cross-linker, initiator, or porogen. Shortly, 2-MBI was mixed with BMK in a 1:1 molar ratio. The voltammetric scan (Appendix Figure D.3 A) showed that with an increasing amount of the

potential sweeps (30>15>4), a better surface insulation of the electrode was obtained. Unfortunately, the baseline during the capacitive measurements was highly unstable and a constant drop in capacitance was observed after PBS purging. This could be explained by an unstable insulation and degradation of the insulation layer. In other cases, when less potential sweeps were applied, it was observed that no significant immobilization occurred (Appendix Figure D.3 B).

In the second approach, the same protocols as for the bulk polymerization were used, while the pre-polymerization mixture was directly brought on the electrode surface and placed under UV or in the oven to start the polymerization. The second protocol will be referred to as the direct polymerization. The pitfall of this technique was the inability to properly wash the obtained particles. Attempts to wash the modified electrode by multiple flushing with the regeneration buffer resulted in a zero-base line during the measurements. This could be explained by the hypothesis that the formed MIPs layer was too thick and was therefore unsuitable for the application.

3.3 MIP performance and characterization

3.3.1 Batch rebinding study by LC-MS/MS

The aim of this test was to determine the influence of the different monomers, cross-linker and the ratio of both compounds on the binding capacity of the MIPs. From the coefficient of the Scatchard analysis (Appendix E), the dissociation constant (K_D) could be calculated, while the apparent maximum binding site (B_{MAX}) was found from the intercept with the y-axis.

Especially one type of synthesized MIPs, consisting of BMK/itaconic acid/vinyl imidazole/ DVB, (1/2/2/6), showed great binding capacity. The K_D and B_{MAX} were determined to be 173.1 nmol mL^{-1} and 114.1 nnmol mg^{-1} respectively. Therefore, these MIPs were chosen as the most promising MIPs towards detection of BMK and were further characterized and validated by the capacitive sensor. Its binding capacity is based on the accumulation of several individual binding interactions between the monomer(s) and/or cross-linking agent with BMK. DVB and 1-vinyl imidazole could interact with the template via π-π interaction between the aromatic systems. Furthermore, the free nitrogen electron pairs of vinyl imidazole and the keto-enol tautomer of BMK are stabilized by hydrogen bonds. Itaconic acid forms hydrophobic interactions between the hydrogen of the hydroxyl moiety of the acid and the aromatic system of BMK. Additionally, the polymer will be functionalized with a carboxyl moiety which can be useful when immobilizing on the gold transducers.

3.3.2 Dynamic light scattering (DLS)

Measurements showed that the selected MIP particles were in the desired range with good homogeneity, 295 ± 45 nm. As a reference, commercially available MIPs towards AMP (MIP technologies, Lund, Sweden), also synthesized by bulk polymerization, were analyzed and showed a similar size of 255 ± 75 nm.

3.3.3 Scanning electron microscopy (SEM) and optical microscopy

Optical microscopy was performed on a gold working electrode before (Appendix Figure F.1A) and after MIP immobilization (Appendix Figure F.1B) using tyramine as a linker and 15 potential sweeps. Picture F.1A shows a bare electrode, the surface is clear and scratch-free. Scratches on the surface would disturb capacitive measurements, therefore special care must be taken for handling of these transducers. The change in colour from yellow to dark yellow-orange was a clear indication of the formation of the polytyramine network which is equally dispersed along the whole surface. The spots on this picture represent aggregates of the MIP particles on the surface but are individually undistinguishable due to their small size. Figure F.1C and F.1D show the SEM pictures of the washed MIP powder. Due to the small size of the particles, it was not possible to immobilize a single layer of the particles and the aggregates were again observed.

3.3.4 Gas chromatography mass spectrometry (GC-MS)

In order to check whether the template was completely removed, tests were performed by GC-MS (Appendix G). At first, MIPs were washed manually by adding MeOH:acetic acid (95:5, v/v) to the MIPs powder. After shaking and centrifugation (5000g, 5 min), the supernatant was removed and new extraction solvent was added. This procedure was repeated for 5 times whereafter the MIPs were dried. GC-MS results showed inefficient template removal since high BMK concentrations were found when adding 1 mL of blank water sample. Therefore, the washing procedure was optimized. MIPs were washed for 48 hours with the same extraction solvent using Soxhlet. After repeating the same GC-MS experiment on the particles washed with the new method, complete template removal was found.

3.3.5 Thermogravimetric analysis (TGA)

Waste water generally has a temperature in the range of 10 to 25°C, depending on the weather, season and local household activities (f.e. shower, laundry). As mentioned in the introduction, the Leuckart reaction takes place at elevated temperatures, from 90-195°C depending on which step of the process takes places. This can drastically affect the temperature of the waste.

Therefore, TGA was performed to investigate the thermal stability of the polymer and as results will show, it is also an easy and fast alternative to check template removal (Appendix H).

A cut-off value of 90% was reached at a temperature of 35.11 and 350.25°C for the unwashed and washed BMK MIPs respectively. In case of unwashed MIPs, unreacted compounds and template degraded at a relatively low temperature causing the drop of the relative weight. The MIP itself started to degrade at a higher temperature. For the MIPs washed by Soxhlet, all unreacted compounds were already removed, therefore only the drop of the polymer degradation was observed. A relative 10% weight loss was only observed at 350.25°C. The commercially available MIPs towards AMP were also analysed as a reference, and a 90% cut-off value was determined at 272.37 °C. Therefore, it can be concluded that the synthesized MIP will be stable during the capacitive measurements, independent of the temperature of the sample.

3.4 Application of the MIPs in a capacitive sensor setup

As the MIPs synthesized by bulk polymerization showed the highest affinity towards the target analyte and direct and *in-situ* polymerisation were inconvenient, an immobilisation step was included to attach the MIP particles on the surface of the gold electrodes. Afterwards, this transducer was placed within the flow cell of the capacitive sensor and affinity, cross-reactivity and pH dependency were investigated.

3.4.1 Immobilization on the gold transducers

MIPs were immobilized by electro-polymerisation using tyramine as a linker. The immobilization was performed for 15 cycli in a potential range from 0 to 1.5V with a scan rate of 0.050 V s^{-1}. The success of this step was checked by CV. The voltammograms before (red curve) and directly after the MIPs immobilization (green curve), and after the final blocking step with 1-dodecanethiol (purple curve) are presented in Figure 1A. After immobilization, the formed layer on the gold electrode decreased the electron exchange resulting in a decrease of the obtained signal. The insulation with 1-dodecanethiol afterwards blocked the remaining active pinholes, and thus only a minimal signal was observed.

The same principle can be applied for the voltammogram of the electropolymerization (Figure 1B). The immobilization was held for 15 cycli in a potential range from 0 to 1.5V with a scan rate of 0.050 V s^{-1}. As the amount of potential sweeps increased, the current response decreased as a thicker layer was created during each step.

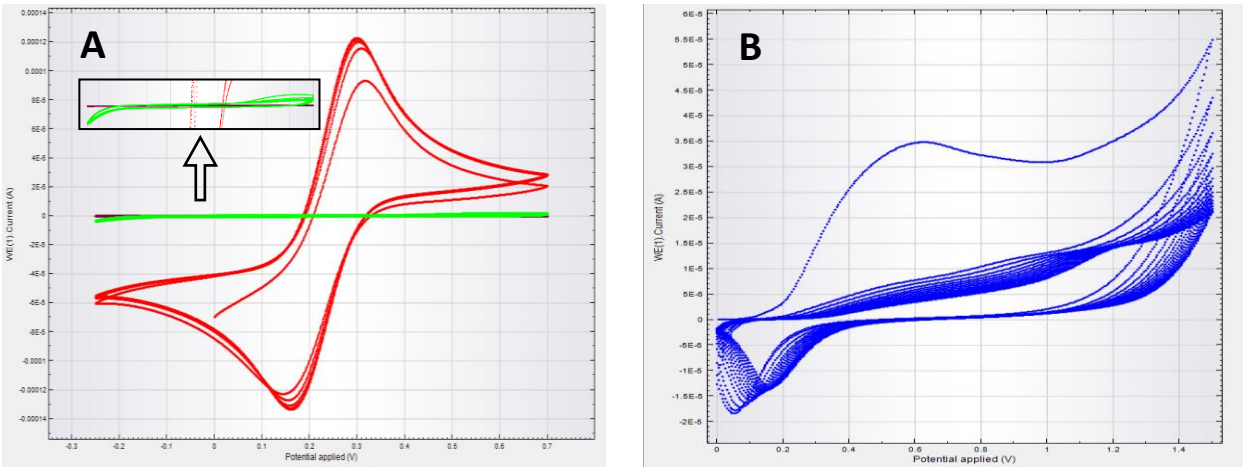

Figure 1A: Cyclic voltammograms before (red), after (green) the MIPs immobilization, and after the final blocking step (pink). 1B: Cyclic voltammograms of the immobilization step. The polymerization was held for 15 potential sweeps in a potential range from 0 to 1.5V with a scan rate of 0.050 V/s. All CV scans were performed in 50 µM $K_3[Fe(CN)_6]$ *in 0.01 mM KCl in a potential range from -0.250 to 0.700 V with a scan rate of 50 mV/s. The gold electrode was the working electrode, a glassy carbon as the auxiliary electrode, and Ag/AgCl as the reference electrode.*

3.4.2 Affinity and cross-reactivity

After MIP/NIP-immobilization, the functionalized electrode was placed in the capacitive sensor. Figure 2A shows the results of the affinity tests where tap water samples spiked with BMK were analysed. A linear range was found from 50 to 1000 µM BMK, the LOD was determined to be 1 µM and the limit of quantification (LOQ) 50 µM in tap water. Blank tap water showed a drop of 0.61 ±0.07 nF, while a capacitive drop of 2.82 ±0.06 nF was found for 1µM BMK in tap water (Appendix I, Figure I.1). Furthermore, the difference in affinity for the MIPs and NIPs is shown. The NIPs represent the non-specific binding towards the target analyte, while the MIP is related to both specific and non-specific bindings. As it can be seen from Figure 2A, the MIP shows an additional affinity towards BMK.

The graph in Figure 2B plots the cross-reactivity of the particles towards structurally related compounds. For this, 250 µM of each cross-reactant was diluted in tap water. The structures of the cross contaminants are presented in SI, Figure 1. The cross-reactivity towards AMP and DPIA was quite low, 22 and 17% respectively. The desired interactions between the selected monomers and the template were H-bonds and π-π stacking. DPIA and AMP both do not have a carboxyl functionality in their structures, only a primary and secondary amine, respectively. Therefore, they cannot have the same type of interaction as BMK with the selected monomers. The MIPs showed a higher cross reactivity (33%) towards NFA due to the similar chemical structure.

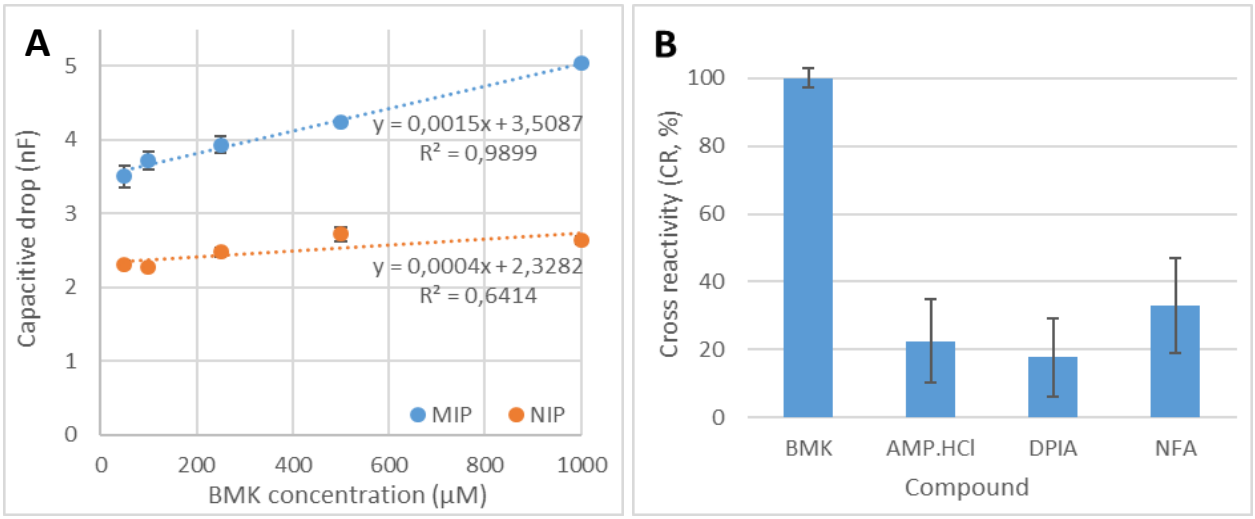

Figure 2A: Affinity test of BMK spiked samples over a wide concentration range for MIP and NIP. 2B: Capacitive change for the MIPs after injection of 250 µM of BMK and other chemically related structures.

As it can be seen in Table 2, the amount of published analytical methods within the last decade towards BMK detection is rather limited. The methods developed by Molgaard et al. (2018) and Di Giovanni et al. (2012) showed great sensitivity towards BMK. Unfortunately, the devices were validated only in standard solutions. Arnoldi et al. (2016) detected BMK in seized samples with headspace gas chromatography (HS-GC/MS) and achieved a working range in mg/g. The presented capacitive sensor is the first electrochemical sensor for BMK, advantaged by its simplicity and minimal sample pre-treatment. Furthermore, the linear range of the developed sensing system is in correspondence with the concentrations found in aqueous samples. In contrary to other research, the focus lays on the monitoring of suspicious ATS-activity and not on the identification of seized powders or the purity of seized samples.

Table 2: Comparison of the analytical techniques and parameters with some of those reported in literature for BMK detection. (Abbreviations: Au, gold; HS-GC/MS, headspace gas chromatography mass spectrometry; MIPs, molecularly imprinted polymers; n.a., not applicable; n.d., not determined; Si, silicon; SiO_2, silicon oxide; Si_3N_4, silicon nitride.)

Reference	**Matrix**	**Method of detection**	**Electrode material**	**Range**	**LOD**
Mølgaard et al., 2018	Pure standard (powder)	Colorimetry combined with gravimetry	SiO_2 and Si_3N_4 surfaces on Si	n.d.	2.0 ag
Di Giovanni et al., 2012	Standard (liquid)	Fluorescence polarization immuno-assay	n.a.	Up to 600 nM	100 nM

Arnoldi et al., 2016	Seized samples	HS-GC/MS	n.a.	1-20 mg/g	n.m.
This work	Water	Capacitance	MIPs immobilized on Au electrodes	10-1000 µM	1 µM

3.4.3 pH dependency

Since the Leuckart reaction takes place at low (step 1) and high (step 2) pH, the pH dependency was investigated by analysing blank and BMK-spiked (250 µM) tap water samples adjusted with 1M HCl or 1M NaOH to different pH values. The selected pH were: 2, 3, 4, 6, 8, 10 and 12. No significant changes in capacitance were found in the pH range of 3-12. Only when the pH reached values lower than or equalling 2 or higher than 12, the measurements were disrupted, and it was no longer possible to calculate the capacitive drop.

3.4.4 Sensor stability, repeatability and reproducibility

As shown in Figure 3, the capacitive sensor shows great stability, with an average baseline of 470.72 ± 0.11 nF and a relative standard deviation (RSD) of 0.047%. The repeatability was checked by the sequential injection (n=10) of 500 µM BMK in water using the same working electrode. The standard deviation (SD) was determined to be 0.221 nF. The reproducibility was checked with a sample concentration of 500 µM BMK in tap water using 10 different electrodes. The SD value of the tested electrodes (n=10) was 0.316 nF. This shows the high reproducibility and repeatability of the proposed technique. Furthermore, it was possible to perform up to 25 analyses before loss of affinity was observed, indicating the sustainability of the developed sensing device.

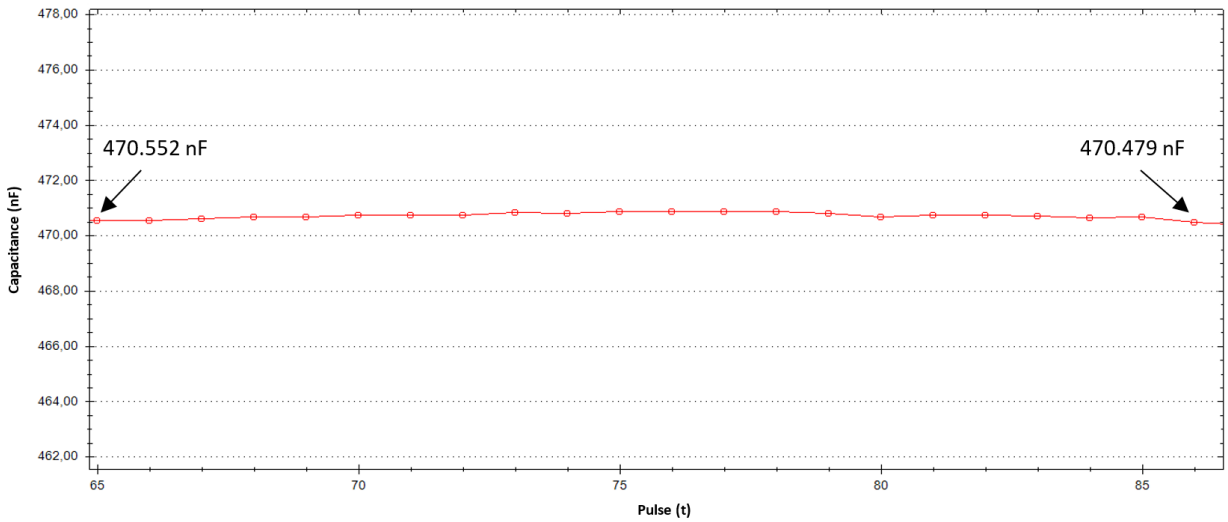

Figure 3: Fluctuation of the baseline (average of 470.720 ± 0.110 nF, RSD 0.047%) of the capacitive sensor.

3.4.5 Validation

The sensor shows an overall good performance when analysing real water samples (Table 3). A strong acidic solution (sample 8) did not have an influence on the analysis. The same can be concluded for medium to strong alkaline solutions of NH_3 and NaOH (sample 3 and 7), and some organic chemicals (sample 7, 12-16). Furthermore, in the applied experimental conditions, no interaction was found between the MIPs and salty solutions (sample 2 and 8). In sample 4 and 9, a low concentration of BMK was falsely found. This can be caused by the cross-reactivity of the MIP towards other ATS markers.

Table 3: Summary of the analyzed samples, matrix: unfiltered tap water. Results were confirmed by LC-MS/MS analysis in-house. The chemical sensor gave a correct or false result**. (Abbreviations: APAAN, alpha-phenylacetoacetonitrile; AMP, amphetamine; BMK, benzyl methyl ketone; DCM, dichloromethane; EtOH, ethanol; HCl, hydrochloride; MeOH, methanol; NaCl, sodium chloride; NaOH, sodium hydroxide; NH_3, ammonia; NFA, N-formyl amphetamine; PBS, phosphate buffered saline; TW, tap water.)*

No.	**Sample content**	**Result of the chemical sensor**	**No.**	**Sample content**	**Result of the chemical sensor**
1*	PBS	Blank	9*	NaOH, pH = 12	Blank
2*	NaCl in TW	Blank	10*	HCl, pH = 3	Blank
3*	NH_3, pH = 10	Blank	11**	APAAN	BMK
4**	NFA and AMP	BMK	12*	EtOH/TW (50/50)	Blank
5*	BMK	BMK	13*	Acetone/TW (50/50)	Blank
6*	Tap water	Blank	14*	Pyridine/TW (50/50)	Blank

7*	Ethyl acetate/ TW (50/50)	Blank	15*	MeOH/TW (50/50)	Blank
8*	$CaCO_3$ in TW	Blank	16*	DCM/TW (50/50)	Blank

4. Conclusions

In the current study, selective MIPs towards the ATS-precursor BMK were synthesized and characterized for the first time, and used as recognition elements in a capacitive sensor. The MIP design was computer-aided using Spartan '16 software. Different polymerization techniques and protocols were compared. Bulk polymerization was found to be the most suitable technique for the desired application, yielding particles in the nanometer range. Batch rebinding studies were performed using LC-MS/MS. It was found that MIPs obtained with 1-vinylimidazole and itaconic acid as monomers and DVB as cross-linker in a template/monomer/co-monomer/cross-linker ratio of 1/2/2/6 revealed the best affinity towards BMK. The final particles were immobilized on the gold electrodes using tyramine as a linker and used for capacitive measurements of BMK in artificially-spiked water samples. The linear range was determined to be 50-1000 µM in tap water, with an LOD of 1 µM. The cross-reactivity towards AMP, NFA and DPIA was 22, 33 and 17% respectively. The overall baseline stability is good, with a standard deviation of 0.22 nF. The repeatability and reproducibility were measured just like the performance in real water samples. In the applied experimental conditions, no interaction was found between the MIP and salty, acidic or alkaline condition. False positives were reported for a combination of NFA and AMP, and APAAN. This is probably caused by the cross contamination of the MIP towards other structurally similar ATS markers. The sensing system showed a great stability, thermal (<350 °C) and pH (3-12) stability, which proves that the developed system can be used for the BMK detection in environmental samples.

Acknowledgement

This work was financially supported by the EU Horizon 2020 Research and Innovation Program under the Grant agreement No 653626 (microMole project) and Fonds Wetenschappelijk Onderzoek (FWO) project 1S67817N. CapSenze Biosystems (Lund, Sweden) is highly acknowledged for their help and support in this work, Bundeskriminalamt (BKA, Wiesbaden, Germany) for the delivery of the standards.

References

Aalberg, L., Andersson, K., Bertler, C., Cole, M.D., Finnon, Y., Huizer, H., Jalava, K., Kaa, E., Lock, E., 2005.

Forensic Sci. Int. 149, 231–241. https://doi.org/10.1016/j.forsciint.2004.06.019

Ahmadi, F., Ahmadi, J., Rahimi-Nasrabadi, M., 2011. J. Chromatogr. A 1218, 7739–7747. https://doi.org/10.1016/j.chroma.2011.08.020

Arenas, L.F., Ebarvia, B.S., Sevilla, F.B., 2010. Anal. Bioanal. Chem. 397, 3155–3158. https://doi.org/10.1007/s00216-010-3865-7

Arnoldi, S., Roda, G., Coceanig, A., Casagni, E., Dell'Acqua, L., Farè, F., Rusconi, C., Tamborini, L., Visconti, G.L., Gambaro, V., 2016. Forensic Toxicol. 34, 411–418. https://doi.org/10.1007/s11419-016-0311-3

Chambers, J.P., Arulanandam, B.P., Matta, L.L., Weis, A., Valdes, J.J., 2002. Receptors, Enzymes, Antibodies, Nucleic Acids, Molecular 1–12.

Couto, R.A.S., Costa, S.S., Mounssef, B., Pacheco, J.G., Fernandes, E., Carvalho, F., Rodrigues, C.M.P., Delerue-Matos, C., Braga, A.A.C., Moreira Gonçalves, L., Quinaz, M.B., 2019. Sensors Actuators, B Chem. 290, 378–386. https://doi.org/10.1016/j.snb.2019.03.138

Darke, S., Kaye, S., Topp, L., 2002. Drug Alcohol Depend. 67, 81–88. https://doi.org/10.1016/S0376-8716(02)00019-4

De Rycke, E., Stove, C., Dubruel, P., De Saeger, S., Beloglazova, N., 2020. Biosens. Bioelectron. 169, 112579. https://doi.org/10.1016/j.bios.2020.112579

Di Giovanni, S., Varriale, A., Marzullo, V.M., Ruggiero, G., Staiano, M., Secchi, A., Pierno, L., Fiorello, A.M., D'Auria, S., 2012. https://doi.org/10.1039/c2ay25772f

Djozan, D., Farajzadeh, M.A., Sorouraddin, S.M., Baheri, T., 2012. Microchim. Acta 179, 209–217. https://doi.org/10.1007/s00604-012-0879-1

Fernández, P., Buján, L., Bermejo, a. M., Tabernero, M.J., 2004. J. Appl. Toxicol. 24, 283–287. https://doi.org/10.1002/jat.994

Gholivand, M.B., Karimian, N., Malekzadeh, G., 2012. Talanta 89, 513–520. https://doi.org/10.1016/j.talanta.2012.01.001

Graniczkowska, K., Pütz, M., Hauser, F.M., De Saeger, S., Beloglazova, N. V, 2016. Biosens. Bioelectron. 1–0. https://doi.org/10.1016/j.bios.2016.09.083

Groeneveld, G., de Puit, M., Bleay, S., Bradshaw, R., Francese, S., 2015. Sci. Rep. 5, 11716. https://doi.org/10.1038/srep11716

Hauser, F.M., Hulshof, J.W., Rößler, T., Zimmermann, R., Pütz, M., 2018. Drug Test. Anal. 10, 1368–1382. https://doi.org/10.1002/dta.2394

Kala, S. V, Harris, S.E., Freijo, T.D., Gerlich, S., 2008. J. Anal. Toxicol. 32, 605–611. https://doi.org/10.1093/jat/32.8.605

Labib, M., Hedström, M., Amin, M., Mattiasson, B., 2010. Anal. Chim. Acta 659, 194–200. https://doi.org/10.1016/j.aca.2009.11.028

Labib, M., Hedström, M., Amin, M., Mattiasson, B., 2009. Anal. Chim. Acta 634, 255–261. https://doi.org/10.1016/j.aca.2008.12.035

Lehrmann, E., Afanador, Z.R., Gallegos, G., Darwin, W.D., Lowe, R.H., 2009. https://doi.org/10.1111/j.1369-1600.2007.00085.x.Postmortem

Lenain, P., De Saeger, S., Mattiasson, B., Hedström, M., 2015. Biosens. Bioelectron. 69, 34–

39. https://doi.org/10.1016/j.bios.2015.02.016

Liu, Y., Hedström, M., Chen, D., Fan, X., Mattiasson, B., 2014. Biosens. Bioelectron. 64, 255–259. https://doi.org/10.1016/j.bios.2014.08.084

Lowdon, J.W., Alkirkit, S.M.O., Mewis, R.E., Fulton, D., Banks, C.E., Sutcliffe, O.B., Peeters, M., 2018. Analyst 143, 2002–2007. https://doi.org/10.1039/c8an00131f

Lurie, I.S., 1997. Application of micellar electrokinetic capillary chromatography to the analysis of illicit drug seizures. J. Chromatogr. A 780, 265–84.

Masteri-Farahani, M., Mashhadi-Ramezani, S., Mosleh, N., 2020. Spectrochim. Acta - Part A Mol. Biomol. Spectrosc. 229, 118021. https://doi.org/10.1016/j.saa.2019.118021

Mølgaard, M.J.G., Laustsen, M., Jakobsen, M.H., Andresen, T.L., Thomsen, E. V., 2018. Sensors Actuators, B Chem. 275, 483–489. https://doi.org/10.1016/j.snb.2018.07.136

Romero Guerra, M., Chianella, I., Piletska, E. V., Karim, K., Turner, A.P.F., Piletsky, S. a., 2009. Analyst. https://doi.org/10.1039/b819351g

Subrahmanyam, S., Piletsky, S.A., 2009. https://doi.org/10.1007/978-0-387-73713-3

Teeparuksapun, K., Hedström, M., Wong, E.Y., Tang, S., Hewlett, I.K., Mattiasson, B., 2010. Anal. Chem. 82, 8406–8411. https://doi.org/10.1021/ac102144a

UNDCP, 1995. the Social Impact. Soc. Dev. 6–12.

United Nations Office on Drugs and Crime, 2017. World Drug Report 2017.

United Nations Office on Drugs and Crime, 2007. World drug report, United Nations Publication. https://doi.org/10.1007/s12117-997-1166-0

UNODC, 2018. World Drug Report. https://doi.org/978-92-1-060623-3

Usami, A., Ohtsu, A., Takahama, S., Fujii, T., 1996. J. Pharm. Biomed. Anal. 14, 1133–1140. https://doi.org/10.1016/S0731-7085(96)01721-9

Vasapollo, G., Sole, R. Del, Mergola, L., Lazzoi, M.R., Scardino, A., Scorrano, S., Mele, G., 2011. https://doi.org/10.3390/ijms12095908

Warner, W. a, Sanchez, R., Dawoodian, A., Li, E., Momand, J., 2013. https://doi.org/10.1111/j.1747-0285.2012.01428.x.Identification

Xiao, D., Jiang, Y., Bi, Y., 2018. Microchim. Acta 185. https://doi.org/10.1007/s00604-018-2735-4

Yao, J., Li, X., Qin, W., 2008. Anal. Chim. Acta 610, 282–288. https://doi.org/10.1016/j.aca.2008.01.042

Zhang, D.W., Zhang, F.T., Cui, Y.R., Deng, Q.P., Krause, S., Zhou, Y.L., Zhang, X.X., 2012. Talanta 92, 65–71. https://doi.org/10.1016/j.talanta.2012.01.049

Zuccato, E., Chiabrando, C., Castiglioni, S., Bagnati, R., Fanelli, R., 2008. Environ. Health Perspect. 116, 1027–1032. https://doi.org/10.1289/ehp.11022

Supplementary information

Appendix A.

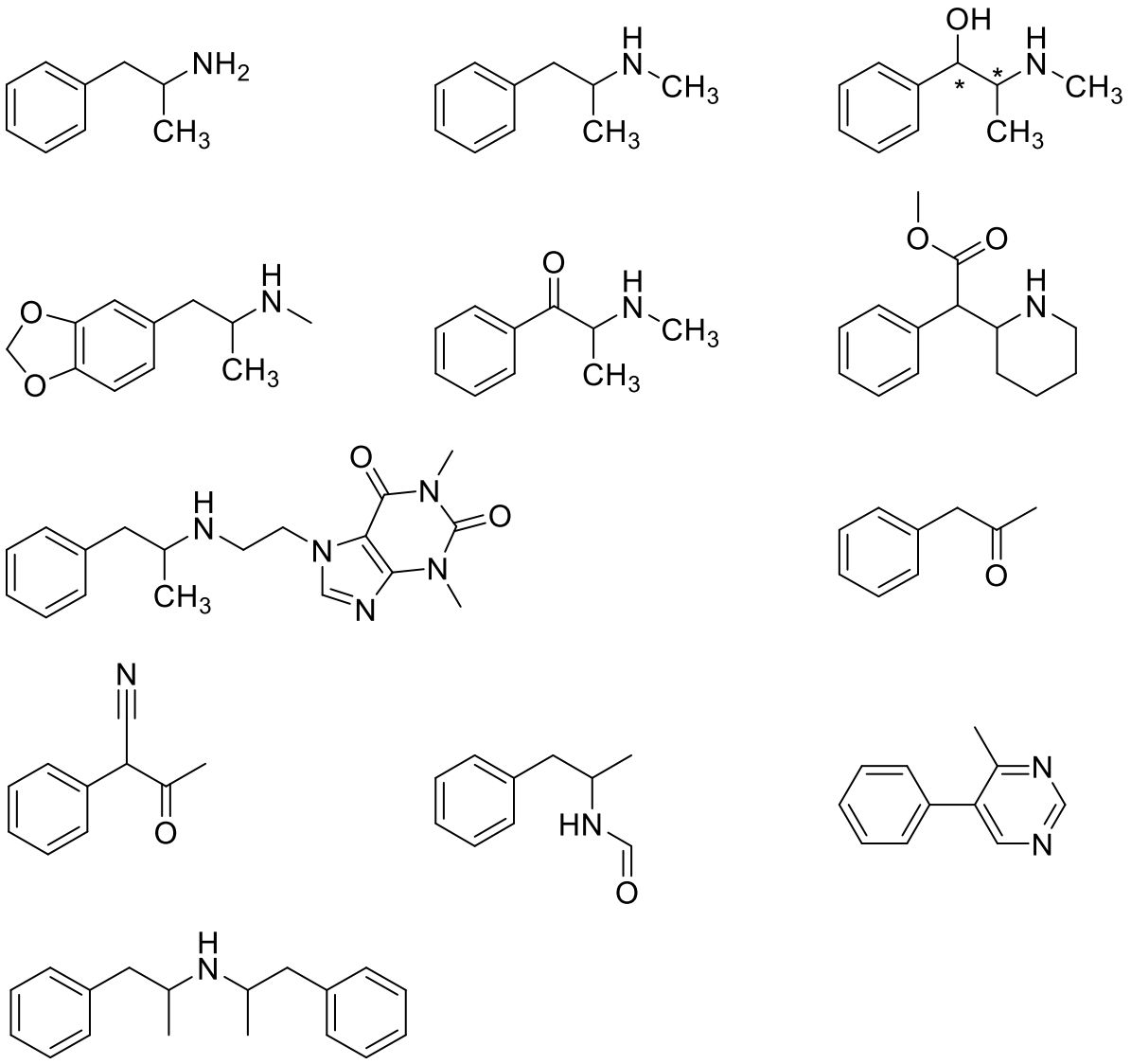

Figure A.1: Chemical structure of the main principal members of the ATS groups, and their derivatives and precursors. From left to right: amphetamine (AMP), methamphetamine (MAMP), and ephedrine (first row); 3,4-methylenedixoymethamphetamine (MDMA), methcathinone, and methylphenidate (second row); fenethylline and benzyl methyl ketone (BMK) (third row); α-phenylacetoacetonitrile (APAAN), N-formyl amphetamine (NFA) *and 4-methyl-5-phenyl pyrimidine (4M5PP) (fourth row); and N,N-*di-(β-phenylisopropyl)amine *(DPIA) (last row).*

Appendix B: Capacitive sensing system

In Figure B.1, pictures are shown of the benchtop and portable capacitive sensors, both present in the host institution. The sensor system consists of two port valves: a 3-port and a 9-port valve. The 3-porte valve is connected via a pump to the running buffer and via an injection loop to the 9-port valve. This valve is connected to the regeneration buffer and the inlet of six samples.

The CapSenze software allows to measure up to 6 samples automatically after each other. Furthermore, both ports have a waste barrel in order to clean the tubings. Regeneration buffer, running buffer and the samples go through an degasser unit with vacuum pump to remove air bubbles which would disrupt the capacitive measurements. The flow cell is the heart of the sensor and holds the functionalized gold transducer. After analyses, all fluidics are collected in a waste barrel. (Figure B.1 right)

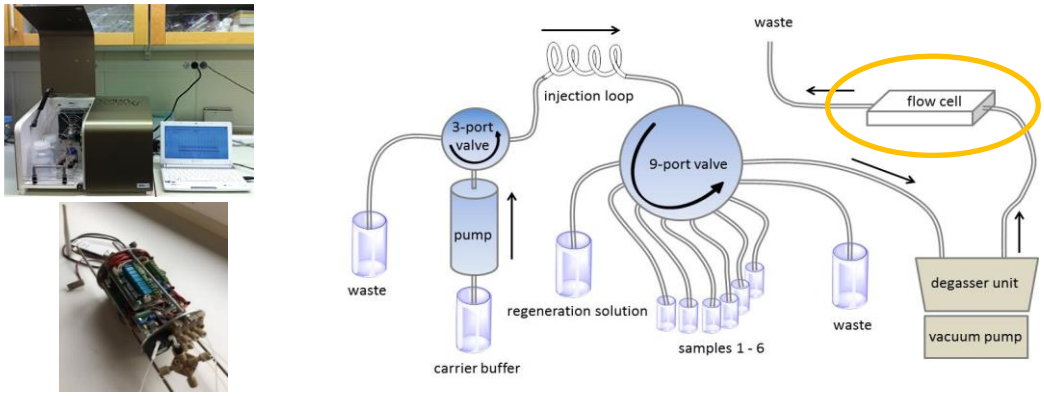

Figure B.1: Picture of benchtop (left top) and portable (left down) capacitive sensor. The right picture shows a schematic overview of the automated flow injection system. The flow cell is the heart of the sensor, holding the functionalized (gold) working electrodes.

Figure B.2 is an example of a typical output of the capacitive analysis. An increase in capacity is found during the regeneration step due to the sudden increase of ions. A drop in capacity is found after sampling due to the binding of the target analyte with the MIP. The size of this drop is directly proportional to the concentration of analyte.

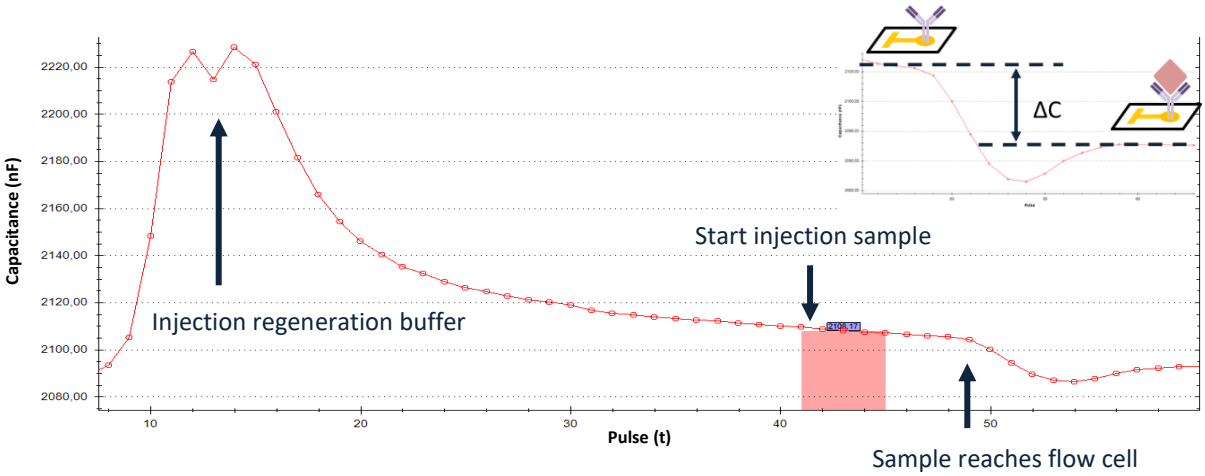

Figure B.2: Typical capacitive measurement, showing the different phases of the analysis scheme, where the capacitance (nF) is plotted in function of time.

Appendix C: Optimization of MIP synthesis through modelling

Table C.1: Binding energies of different monomers and cross-linking agents and the template benzyl methyl ketone (BMK), in a molar ratio of 1:1. Cross-linkers are assigned with an asterisk, the most promising monomers and cross-linkers are indicated in bold.

Binding energy between template and monomer or cross linker*(kJ mol^{-1})			
1-vinylimidazole (VI)	**-17.92**	allylamine	3.65
2-vinylpyridine	38.23	uroganic acid ethyl ester	-10.86
acrylamido-2-methyl-1-propanesulfonic acid	184.44	**itaconic acid (IA)**	**-18.19**
2-hydroxyethylmethacrylate (HEMA)	-9.156	methacrylic acid	-14.73
4-vinylpyridine	3.06	**styrene (STY)**	**-26.29**
acrolein	-0.50	uraganic acid	1.22
acrylamide	2.74	*N*,*N*-diethylamino ethyl methacrylate	9.95
acrylic acid	1.27	*N*-phenylacrylamide	10.43

acrylonitrile	2.98	**p-divinylbenzene (DVB)***	**3.28**
ethylene glycol dimethacrylate (EGDMA)*	**2.72**	methylene-bis-acrylate*	-5.38
trimethylolpropane trimethacrylate (TRIM)*	2.62	pentaerythritol tetra-acrylate (PETRA)*	2.41

Appendix D: Detailed protocols for MIP synthesis towards BMK

D.1 Emulsion polymerization

First, a disperse phase (organic) and a continuous phase (aqueous) were prepared separately. The former phase consisted of 278 mg AIBN dissolved in 10 mL chloroform. The latter one consisted of 101 mg PVA (Mw 146.000-186.000, 99+% hydrolysed) as an emulsion stabilizer, in 20 mL water. Two molar ratios of template BMK: functional monomer: cross-linker, 1/4/16 and 1/4/20, were tested and compared. The different tested compounds can be found in Table 1. These compounds were mixed for 30 s at 15 000 rpm together with 0.9 mL dispersive phase and 4.7 continuous phase. After flushing with nitrogen, the flask was sealed off and placed between UV lights (λ = 365 nm; 150 mW cm^{-2}) while stirring at 250 rpm. The polymerization was held for 2h at room temperature. In order to synthesize MIPs with smaller size, the last two protocols were repeated except that polymerization only took place for one hour.

Table D.1: Different compounds and ratios tested during emulsion polymerization.

Template	**Functional monomer**		**Cross-linker**	**Ratio**
BMK	Styrene		EGDMA	1:4:16 and 1:4:20
	1-vinylimidazole		DVB	1:4:16 and 1:4:20
	Styrene	Itaconic acid	EGDMA	1:2:2:20
	1-vinylimidazole	Itaconic acid	DVB	1:2:2:20
	Styrene	1-vinylimidazole	DVB	1:2:2:20
	Styrene	1-vinylimidazole	EGDMA	1:2:2:20

The template was removed by rinsing the MIPs for 16h with an MeOH/acetic acid solution (95:5) in a Soxhlet extractor. The obtained particles were characterized by DLS and immobilized on gold electrodes for capacitive analysis.

The MIPs consisting of 1-vinylimidazole, itaconic acid and DVB in a ratio 1:2:2:20 were immobilized on gold electrodes for subsequent capacitive analysis. As it can be seen in Figure D.1, an unstable baseline with values between 0 and 1400 nF was found.

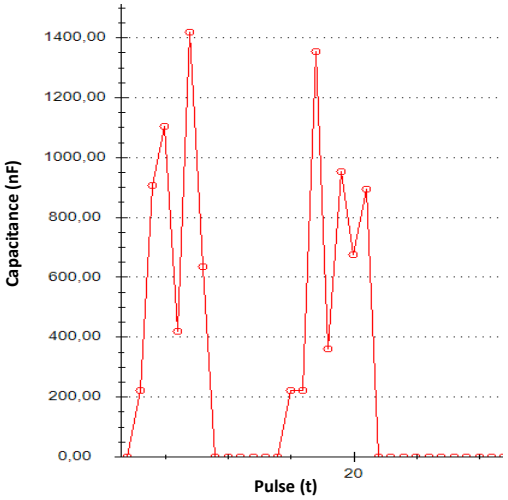

Figure D.1: Capacitive baseline of functionalized gold electrode with emulsion MIPs, consisting of 1-vinylimidazole, itaconic acid and DVB in a ratio 1:2:2:20.

D.2 Bulk polymerization

Fifty mg of AIBN were dissolved in the porogen, DMF (2.65 mL). The template (BMK), and the selected functional monomers (itaconic acid, styrene, and 1-vinylimidazole) were added according to Table 2. After sonication for 5 minutes, the cross-linking agent (DVB, EGDMA) was added. Different molar ratios of template/functional monomer/co-monomer/cross-linker were tested, such as 1/2/2/6, 1/2/2/16, and 1/2/2/20. The pre-polymerization mixture was flushed with nitrogen for 5 minutes and sealed off. Polymerization occurred under UV light (λ = 365 nm, 150 mW cm^{-2}) for 20 minutes and subsequently heated at 80°C for 3h in an oil bath. The monolith was crushed and sieved wetly. The template was removed by rinsing the obtained MIPs for 16h with an MeOH/acetic acid (95/5, v/v) solution in a Soxhlet extractor. Non-imprinted polymers (NIPs) were synthesized via the same protocols, but in absence of the template. The obtained particles were characterized by optical microscopy, TGA, SEM, DLS GC-MS and LC-MS/MS.

D.3 *In-situ* and direct polymerization

Electropolymerization has been used in the development of several MIPs-based chemosensors(Couto et al., 2019; Crapnell et al., 2019), including a few capacitive

sensors(Gong et al., 2004; Najafi & Baghbanan, 2012; Wang et al., 2007), and this idea became interesting since no initiator, cross-linker, or porogen are needed. Moreover, MIPs are synthesized directly on the surface, and no linker is necessary as well. A poly-(2-mercaptobenzimidazole) film (PMBI) used for this polymerization approach, as it is chemically inert and stable under extreme conditions. Looking at the structure of 2-MBI monomer (Figure D.2), the sulphur atom from the thiohydroxyl group could easily bind with the gold surface of an electrode, and its aromatic system could form a π-π stacking with the aromatic ring of BMK.

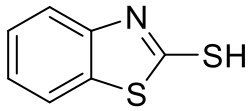

Figure D.2: Chemical structure of 2-mercaptobenzimidazole (2-MBI).

2-MBI (50 mM solution was prepared in EtOH/H_2O (70/30, v/v) at pH 10 by adding NaOH) and BMK (10 mM solution in EtOH) were mixed in a molar ratio of 1/1. 300 µL of this mixture were brought in a galvanic cell. Electropolymerization was performed from 0.6 V to 1.5 V using a potential step of 0.01 V s^{-1}. Different amount of potential sweeps were compared. (A: 4, B: 15, and C: 30) (Figure D.3). Based on literature, a fourth procedure was tested where 50 mM 2-MBI in EtOH and 7 mM of BMK in EtOH were brought together in ratio 1/1 and polymerization was performed for 8 potential sweeps from -0.6 to 1.3V with a scan rate 1 V s^{-1}. The functionalized electrode was washed within the capacitive sensor by an excess of regeneration buffer. CV was performed in 50 µM $K_3[Fe(CN)_6]$ in 0.01 mM KCl in a potential range from -0.250 to 0.700 V with a scan rate of 50 mV s^{-1}. The gold electrode was the working electrode, a glassy carbon –as auxiliary electrode, and Ag/AgCl – reference electrode.

In-situ polymerization was performed directly on the surface of an electrode without any linker between the gold surface and the particles. A drop (20 µL) of a pre-polymerization mixture (the same as used for bulk polymerization) was brought on a bare, cleaned gold electrode. Thermal polymerization was performed in an oven for 2h at 65°C. The functionalized electrode was washed within the capacitive sensor by an excess of regeneration buffer.

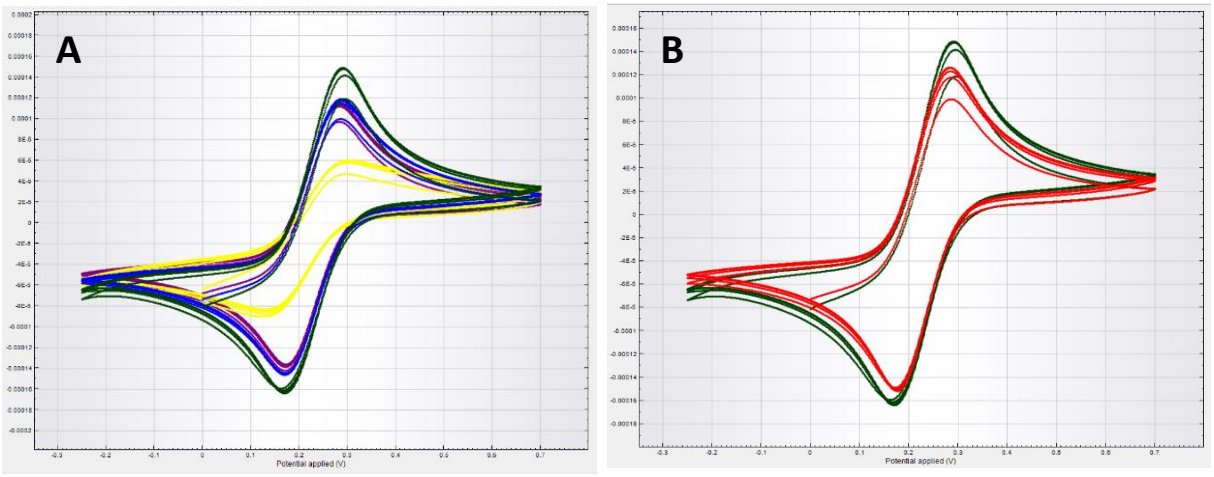

Figure D.3: A: Cyclic voltammogram (CV) of a bare electrode (green) and the same electrode after in-situ polymerization with 4 (blue), 15 (yellow), and 30 (purple) potential sweeps (left). B: CV before (green) and after (red) immobilization using the fourth protocol.

Appendix E: Batch rebinding study by LC-MS/MS

The overall performance of the polymers was investigated during a batch rebinding study (equilibrium experiment), based on LC-MS/MS analysis. Using Scatchard analysis; the dissociation constant K_D and apparent maximum binding site B_{MAX} were calculated.

Analysis were performed using an Acquity UPLC system coupled to a Waters Xevo® TQ-S triple quadrupole mass spectrometer (Waters Technologies, Zellik, Belgium). Chromatographic separation was performed by an Acquity UPLC® HSS T3 (1.8 µm x 2.1 x 100 mm) column (Waters, Milford, MA, USA). The temperature of the column and autosampler was set at 40 °C and 10 °C, respectively. A modified procedure for the gradient elution was established based on Vazquez et al.(Vazquez-Roig et al., 2010), with a flow rate of 0.4 mL min^{-1}, an injection volume of 10 µL, resulting in a total run time was 7 minutes. Masslynx and Targetlynx software 4.1 (Waters Corp., Milford, MA, USA) were used for the data acquisition and processing). BMK was found at a retention time of 5.20 min. The MS analyses were carried out using multiple reaction monitoring (MRM) with a positive electrospray ionization (ESI+).

Five mg MIP/NIP were transferred in an Eppendorf tube and spiked with 1 mL of different BMK concentrations (diluted in water) in the range of 0 to 1000 µM. The tubes were vortexed, shaken overnight (16h), and afterwards centrifuged for 5 minutes at 14 000 g. The supernatants were collected and directly analysed by LC-MS/MS. The amount of bound BMK was calculated as the difference between the initial spike concentration and the concentration of the template present in the supernatants after equilibrium, which represents the free BMK concentration. The

binding isotherms were translated by the use of the Scatchard equation into the linear equations, according to:

$$\frac{B}{[F]} = \frac{B_{MAX} - B}{K_D}$$

Where B is the amount of bound template, [F] the concentration of free template in solution, B_{MAX} the apparent maximum number of binding sites, and K_D the dissociation constant.

Appendix F: Scanning electron microscopy and optical microscopy

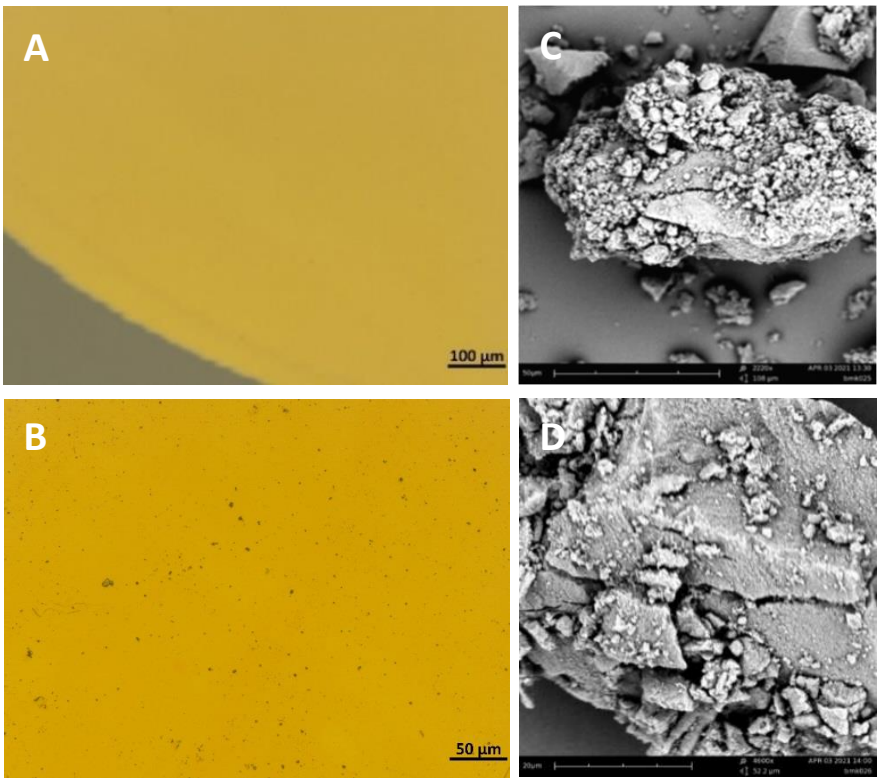

Figure F.1: Optical microscopy pictures of a bare gold electrode (A) and a gold electrode after MIP-tyramine functionalization (B). SEM pictures of the optimized MIP particles (C and D).

Appendix G: GC-MS/MS analysis

The efficiency of the washing procedure on the MIPs towards BMK were tested by GC-MS.

G.1 GC-MS Method

GC-MS analysis were performed using an GC-MS Triple Quadrupole 7890B/7000C system of Agilent Technologies Company (Santa Clara, California, USA). Chromatographic separation was obtained using a capillary HP5MS column (length 30 m, diameter 0.25 mm, and film thickness of 0.25 µm) and a pre-column with a length of 3 m, diameter of 0.25 mm, and film thickness of 0.10 µm. The programme was set as followed: after holding 1 min at 70 °C, the

temperature was raised at a speed of 5°C min^{-1} to 120°C and again held for 1 min. Afterwards the temperature raised to 300°C at a rate of 15°C min^{-1} and held for 1 min. 1µL of volume was injected, helium gas was purged at a speed of 1.2 mL min^{-1}. The initial temperature for the MS-detector was set on 310 °C, scans were performed from 40 to 300 m/z.

In order to test the efficiency of our washing procedure, 1 mL of pure water was added to different MIP samples with known weight (approximately 5 mg). After shaking overnight at 4 °C, 100 µL of supernatant solution was collected, and extracted with 1 mL of toluene containing the internal standard (ISTD) nonadecane. 200 µL was injected and analysed by the above mentioned GC-MS method. This is referred to as the BMK concentration in "solution" (supernatant). In the next step, the solution were decanted from the MIPs and bound BMK was extracted from the MIPs by adding 1 mL toluene with ISTD and mixed and centrifuged (5 min at 14 000 g) afterwards. 200 µL of this supernatant was injected and analysed by the above mentioned GC-MS method. This is referred to as the BMK concentration of "MIPs" since this is the BMK concentration which was bound to the MIPs. If the washing procedure is efficient, no or low concentration of BMK should be found.

G.2 GC-MS Results

As it can be seen from Figure G.1, high BMK concentration can still be found for the MIPs, who were washed manually (M1-M6). Therefore, this washing procedure is found inefficient. Instead when looking at the MIPs washed for 16h with Soxhlet (S1-2), no BMK was found neither in the supernatant or bound to the MIPs. Therefore, this washing procedure will be applied for further tests.

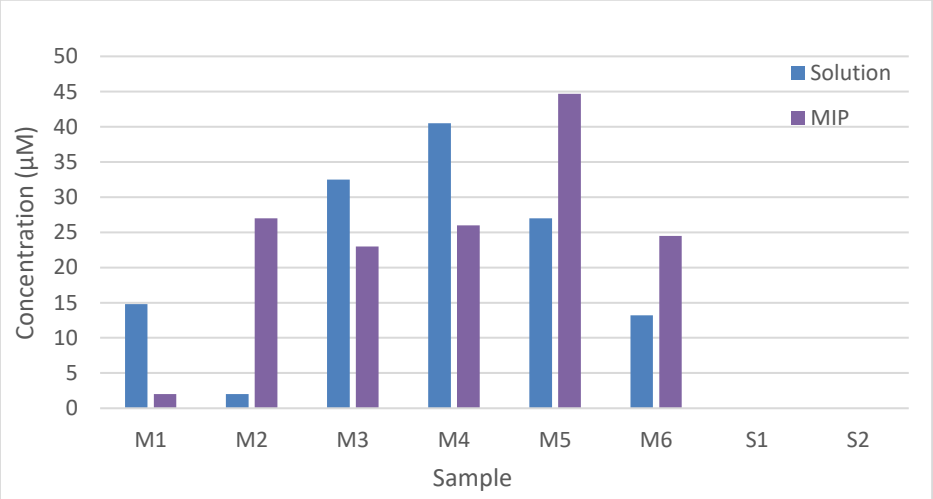

Figure G.1: BMK concentration in function of the different MIP samples, washed by different procedures. "M" refers to manual washing while "S" stands for Soxhlet.

Appendix H: TGA analysis

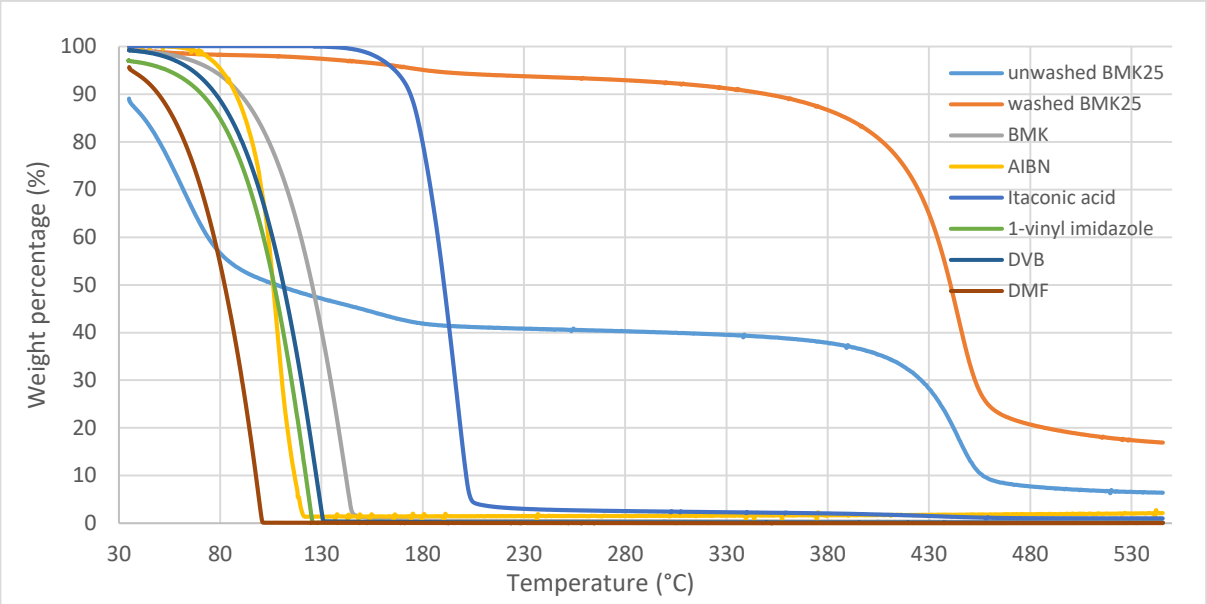

Figure H.1: TGA analysis of the washed and unwashed synthesized MIPs and of the different compounds used during the production process.

Appendix I: Affinity tests

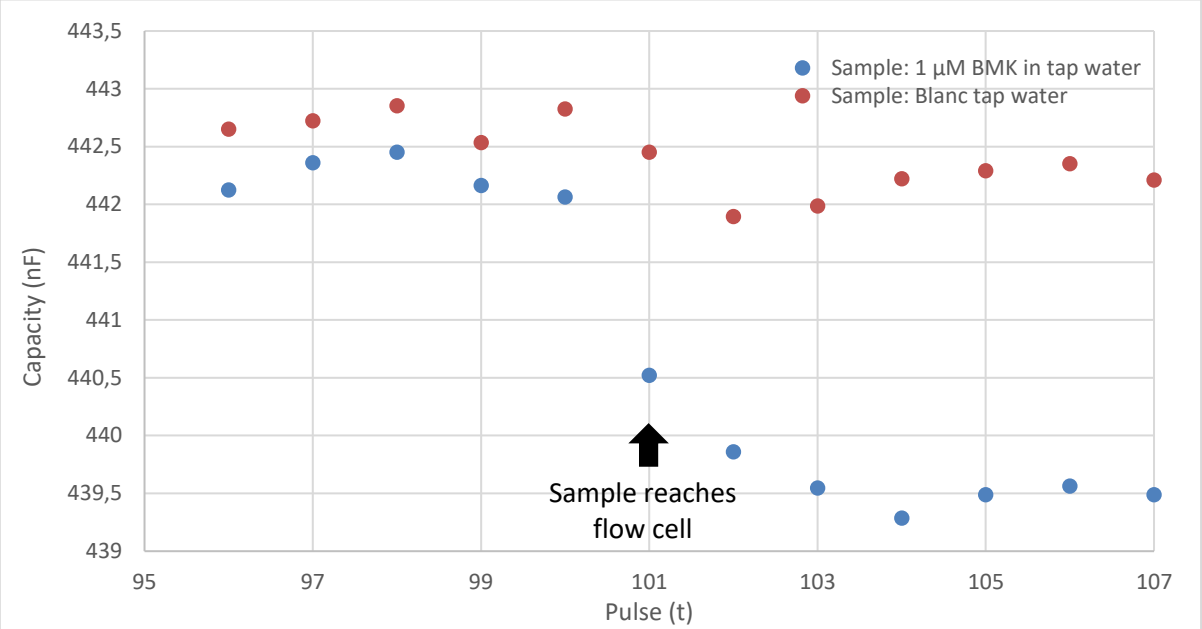

Figure I.1: Capacitive response for 1 µM BMK in tap water (LOD) versus blank tap water.

Table 2: Capacitive drop for 1 µM BMK in tap water (LOD) and blank tap water, analyses performed in triplicate.

Sample	Capacitive drop (nF)	Sample	Capacitive drop (nF)
Blank Sample 1	0,423	Sample 1 (1 µM)	2,805
Blank Sample 2	0,660	Sample 2 (1 µM)	2,675
Blank Sample 3	0,748	Sample 3 (1 µM)	2,968
Average	**0,610**	**Average**	**2,816**
Standard deviation	**0,137**	**Standard deviation**	**0,120**

References

Couto, R. A. S., Costa, S. S., Mounssef, B., Pacheco, J. G., Fernandes, E., Carvalho, F., Rodrigues, C. M. P., Delerue-Matos, C., Braga, A. A. C., Moreira Gonçalves, L., & Quinaz, M. B. (2019). *Sensors and Actuators, B: Chemical*, *290*, 378–386. https://doi.org/10.1016/j.snb.2019.03.138

Crapnell, R. D., Hudson, A., Foster, C. W., Eersels, K., van Grinsven, B., Cleij, T. J., Banks, C. E., & Peeters, M. (2019). *Sensors (Switzerland)*, *19*(5). https://doi.org/10.3390/s19051204

Gong, J. L., Gong, F. C., Kuang, Y., Zeng, G. M., Shen, G. L., & Yu, R. Q. (2004). *Analytical and Bioanalytical Chemistry*, *379*(2), 302–307. https://doi.org/10.1007/s00216-004-2568-3

Najafi, M., & Baghbanan, A. A. (2012). *Electroanalysis*, *24*(5), 1236–1242. https://doi.org/10.1002/elan.201100687

Vazquez-Roig, P., Andreu, V., Blasco, C., & Picó, Y. (2010). *Analytical and Bioanalytical Chemistry*, *397*, 2851–2864. https://doi.org/10.1007/s00216-010-3720-x

Wang, Z., Kang, J., Liu, X., & Ma, Y. (2007). *International Journal of Polymer Analysis and Characterization*, *12*(2), 131–142. https://doi.org/10.1080/10236660601140821